



Gold-decorated magnetic nanoparticles modified with hairpin-shaped DNA for fluorometric discrimination of single-base mismatch DNA

Mei-Hwa Lee¹ · Ching-Chich Leu² · Cheng-Chih Lin³ · Yu-Fan Tseng² · Hung-Yin Lin^{2,4} · Chia-Ning Yang^{5,6} 

Received: 3 December 2018 / Accepted: 15 December 2018 / Published online: 9 January 2019
© Springer-Verlag GmbH Austria, part of Springer Nature 2019

Abstract

The authors describe the use of gold-decorated magnetic nanoparticles (Au/MNPs) in discriminating DNA sequences with a single-base (guanine) mismatch. The Au/MNPs were characterized through dynamic light scattering, X-ray diffraction, superconducting quantum interference device, and UV/visible spectroscopy. They were then conjugated to a probe oligomer consisting of a hairpin-shaped DNA sequence carrying two signalling fluorophores: fluorescein at its 3' end and pyrene in the loop region. When interacting with the target DNA sequences, the hybridized probe–target duplex renders the pyrene signal (at excitation/emission wavelengths of 345/375 nm) either quenched or unquenched. Quenching (or nonquenching) of the pyrene fluorescence depends on the presence of a guanine (or a nonguanine) nucleotide at the designated polymorphic site. The linear range of hybridization in these Au/MNPs is from 0.1 nM to 1.0 μM of ssDNA. Conceivably, this system may serve as a single-nucleotide polymorphism probe.

Keywords Gold-decorated magnetic nanoparticles · DNA sequences · Single-base mismatch

Introduction

Nanoparticles (NPs) of noble metals have received great attention because of their electronic, optical, and thermal properties [1]. In particular, gold (Au) NPs are used in many fields because of their unique structural, electronic, optical, and catalytic characteristics [2, 3]. In addition, Au-NPs can be conjugated with many functionalizing agents, including polymers, surfactants, ligands, dendrimers, drugs, DNA, RNA, proteins, peptides, and oligonucleotides [3]. Their multiple surface functionalities render Au-NPs a versatile platform

for a broad range of applications. Because of the high biocompatibility of Au-NPs, great progress has been made in their biomedical use in biosensors, therapies, diagnosis, and clinical chemistry, such as immunoassays, genomics, cancer cell photothermolysis, microorganism detection and control, targeted drug delivery, and optical imaging for monitoring biological cells and tissues through resonance scattering or in vivo photoacoustic techniques [3, 4].

The synthesis, surface functional strategies, and biomedical applications of magnetic nanoparticles (MNPs) were extensively reviewed by Wu et al. [5]. A mixture of ferric and

Electronic supplementary material The online version of this article (<https://doi.org/10.1007/s00604-018-3192-9>) contains supplementary material, which is available to authorized users.

✉ Hung-Yin Lin
linhy@nuk.edu.tw

✉ Chia-Ning Yang
cnyang@nuk.edu.tw

¹ Department of Materials Science and Engineering, I-Shou University, Kaohsiung 84001, Taiwan

² Department of Chemical and Materials Engineering, National University of Kaohsiung, Kaohsiung 81148, Taiwan

³ Division of Pulmonary Medicine, Department of Internal Medicine, Armed-Forces Zuoying General Hospital, Kaohsiung 81342, Taiwan

⁴ Department of Chemical and Materials Engineering, National University of Kaohsiung, 700, Kaohsiung University Road, Nan-Tzu District, Kaohsiung 811, Taiwan

⁵ Department of Life Sciences, National University of Kaohsiung, Kaohsiung 81148, Taiwan

⁶ Department of Life Sciences, National University of Kaohsiung, 700, Kaohsiung University Road, Nan-Tzu District, Kaohsiung 811, Taiwan

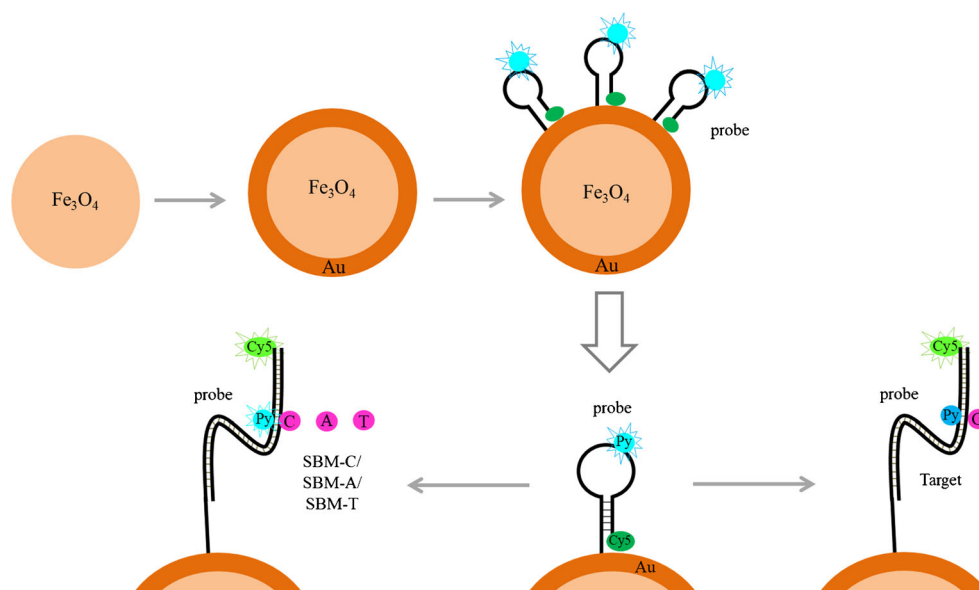
ferrous ions was coprecipitated in 1:2 M ratio under extremely basic solutions at room or elevated temperature. We previously demonstrated the applications of MNPs [6–10], in which molecularly imprinted polymers (MIPs) were coated on MNP surfaces and used for extracting biomolecules [6, 8], immobilizing enzymes [7], and DNA/drug therapy [8–10]. For instance, resveratrol from Chinese medicine extracts was used for suppressing human osteogenic sarcoma [8]. Amylase can be immobilized on magnetic MIPs for starch hydrolysis [7]. Moreover, molecularly imprinted chitosan-coated MNPs can be used for gene delivery [10] and protein activation in cancer cell treatment [9].

Three basic types of Au-NP and MNP combinations are used: the first two have either Au or magnetic material in the core and another material in the shell, namely Au@Fe₃O₄ and Fe₃O₄@Au [11], whereas the third is the Au–Fe₃O₄ dumbbell NP. Monodispersed core–shell Fe₃O₄@Au NPs were first reported by Wang et al. [11]. Iron (III) acetylacetonate and Au acetate were dissolved in phenyl ether and sequentially added after reduction using 1,2-hexadecanediol [11]. Core–shell and dumbbell-like NPs were also used to label radioactive [^{99m}Tc(CO)₃]⁺ moiety on an Au surface [12]. Sun et al. reported tunable plasmonic properties [13] and Magnetic Resonance Imaging (MRI) analyses [14] of the core–shell and dumbbell NPs. Nguyen et al. [15] and Gun'ko et al. [16] reviewed the synthesis, characterization, and biomedical applications of Au and magnetic composite NPs. The applications of magnetoplasmonic heteronanostructures [15, 16] include imaging [14], therapy [17], biosensors [18], and SERS [19]. Although Au–Fe₃O₄ NPs have been investigated for their production mechanism, Au@Fe₃O₄ NPs have mainly been examined for their high MRI intensity, methyl orange catalysis [20], C(sp²)–H activation [21], and nitroarenes [22].

Moreover, the enhancement of the surface plasma resonance (SPR) effect [19] typically requires the exposure of the NP Au surface; therefore, Fe₃O₄@Au can be used in sensing DNA [23]. Au–Fe₃O₄ NP synthesis has been used to form DNA complexes for sensing target DNA sequences, with a sensing range from 0.1 fM to 1.0 μM for complementary DNA sequences [23].

A DNA-based single-nucleotide polymorphism (SNP) probe was mounted on Au-decorated MNPs (Au/MNPs) for discriminating guanine (G) and non-G nucleotides at a designated site. These NPs were synthesized with MNPs as the core to which a HAuCl₄ solution was added; the Au ions were reduced to Au-NPs and deposited on MNPs. During preparation, the Au/MNPs were characterized through dynamic light scattering (DLS), X-ray diffraction (XRD), superconducting quantum interference devices (SQUID), and UV/visible spectroscopy. The probe sequence (Table 1) is a 41-nucleotide (41-nt) molecular beacon [24], with a 25-nt loop, 8-nt stem, and a pyrene-hooked pyrrolocytidine [marked as C*] labeled in the loop region. The 3' end of the stem carries a fluorescein; by contrast, rather than a quencher labeling, the 5' end is labeled by disulfide (marked as C6-thiol) for Au surface immobilization such that the fluorescein emission can be quenched by the nearby Au when the probe stays in hairpin conformation. In Scheme 1, the upper panel illustrates the Au/MNP fabrication, and the lower panel demonstrates the SNP detection working principle. When the probe sequence is attached to the Au/MNP, its hairpin conformation causes the fluorescein emission to be quenched by Au surface; however, the pyrene emission is observable. However, interacting with the added target sequence, target–probe duplex formation shifts fluorescein away from the Au surface, whereby the fluorescein emission becomes observable.

Scheme 1 Schematic presentation of probe-conjugated Au/MNP preparation (upper panel) and working principle to discriminate DNA with or without single-base (guanine) mismatch sequences at the polymorphic sites (lower panel). Py denotes pyrene-hooked pyrrolocytidine; F denotes fluorescein



Experimental

Reagents

All the oligonucleotides listed in Table 1 were purchased from Yao-Hong Biotechnology Inc. (HPLC grade; New Taipei City, Taiwan; <http://www.yh-bio.com.tw/>). Iron (III) chloride 6-hydrate (97%), iron (II) sulfate 7-hydrate (99.0%), trisodium citrate (ACS grade), and sodium borohydride (NaBH₄, 98.0%) were purchased from Sigma-Aldrich Chemical Company (St. Louis, MO, USA; <https://www.sigmaaldrich.com/>) and Panreac (Barcelona, Spain; <http://www.panreac.es/>). Sodium chloride (AR grade), potassium chloride, potassium dihydrogen phosphate (KH₂PO₄ > 99.9%), and sodium phosphate dibasic (Na₂HPO₄ > 99%) were purchased from J. T. Baker (Phillipsburg, NJ, USA; <http://jtbaker.com/>). Hydrogen tetrachloroaurate trihydrate (HAuCl₄·3H₂O, 99.9%) and (3-aminopropyl)triethoxysilane (APTES, 99%) were from Alfa Aesar (Haverhill, MA, USA; <https://www.alfa.com/>) and Acros (NJ, USA; <https://www.acros.com/>), respectively. The deionized water used for preparing phosphate-buffered saline (PBS; containing 110 mM NaCl, 2 mM KCl, 8 mM Na₂HPO₄, and 2 mM KH₂PO₄, pH 7.4) and rinse solutions had resistivity of 18.2 MΩ·cm and was prepared using Purelab Ultra (Elga Lab-Water, Albania; <http://www.elgalabwater.com/>). All purchased chemicals were used as received, unless noted otherwise.

Au/MNP synthesis

The MNPs were synthesized using the Massart method, which entailed coprecipitation of a mixture of iron (III) chloride 6-hydrate and iron (II) sulfate 7-hydrate by using sodium hydroxide. The magnetite was washed and then freeze dried overnight. To prepare the core-shell Au/MNPs with an ultrathin Au shell, Au-NPs with a particle size of less than 5 nm were attached to MNP surface. Au-NPs were synthesized through NaBH₄ reduction of HAuCl₄·3H₂O in an ice bath [25]. A 20-mL ice-cold aqueous solution containing 1 mM HAuCl₄ and 38.8 mM trisodium citrate was prepared in a

beaker. To this solution, 0.6 mL of 0.1 mM NaBH₄ solution was quickly added with vigorous stirring. The color of the solution changed from pale yellow to wine red. We used an effective self-assembly method to construct the core-shell Au/MNPs with APTES as the mediator. Based on its two-end functional groups, APTES can bind concurrently to the oxide surface of MNPs (Si(OH)₃ side) and the metal surface of Au-NPs (NH₂ side). MNP solution (2 mL) and APTES (0.18 mL) were separately added to 50 mL of ethanol and homogenized with a magnetic stirrer at 500 rpm for 1 h. The solution was then heated to 100 °C and stirred at 500 rpm for 2 h to assist APTES molecules in bonding to the MNPs and forming an aminated surface. The APTES-modified MNPs were then collected using a strong magnet, the supernatant was discarded, and the collected NPs were dispersed in the same volume of ethanol through sonication. This rinsing process was repeated five times to remove residual APTES molecules, and then, the NPs were redispersed through sonication in 10 mL of ethanol. Subsequently, 3 mL of the APTES-modified MNP solution was added to 9 mL of Au-NP solution and stirred at 450 rpm for 5 h. When the MNP solution was added to the Au-NP solution, electrostatic interactions between amides and Au-NPs led to adsorption. Au-NP surface carries a negative charge density because of the presence of absorbed citrate ions. Because aminated surfaces are positively charged (pKa of the surface = ~9; pH of the solution = ~9) [26], Au-NPs absorb to this surface to form the core-shell Au/MNPs. The synthesized NPs were collected using a strong magnet and rinsed once with ethanol and four times with deionized water to remove free Au-NPs. Finally, the NPs were redispersed using sonication in 3 mL of deionized water.

Au/MNPs characterization

The prepared Au/MNPs and DNA probe-conjugated Au/MNPs thus were monitored using a DLS particle sizer (90Plus; Brookhaven Instruments Co., New York, USA; <https://www.brookhaveninstruments.com/>). The measurement of the particle size distribution was set at 25 °C with 3-min data collection at a 90° detection angle. The average background count rate was 15 kcps, whereas that

Table 1 DNA sequences used in this study

	DNA Sequence
Probe	5' (C6-thiol) GCAGTGCTGACGTCTCACTC*AGCAGTCACTAGCAGCACTGC fluorescein 3'
Target	5' GCTAGTGACTACTGAGTGAGACGTC 3' fully matched
SBM-C	5' GCTAGTGACTACTCAGTGAGACGTC 3' base-C mismatched
SBM-A	5' GCTAGTGACTACTAGTGAGACGTC 3' base-A mismatched
SBM-T	5' GCTAGTGACTACTTAGTGAGACGTC 3' base-T mismatched

C* in the probe sequences denotes pyrene-hooked pyrrolocytidine

The underlined bases in target sequences specify the polymorphic site

The 5' end of the probe sequence was modified with C6 thiol for immobilization on the Au surface

of each measurement was between 20 and 500 kcps. XRD analysis (D8 Advance XRD; Bruker, Germany; <http://www.kratos.com/>) was used to determine the crystalline structure of the Au/MNPs with Cu K α radiation of $\lambda = 1.5406 \text{ \AA}$. SQUID uses highly sensitive magnetometers to measure extremely small magnetic fields based on superconducting loops containing Josephson junctions. The magnetization of MNPs and Au/MNPs was measured for magnetic properties using the MPMS XL-7 system (Quantum Design, San Diego, CA, USA; <https://www.qdusa.com/>) at 298 K in $\pm 15,000 \text{ G}$. All spectral and absorbance measurements of NP solutions were carried out using a PerkinElmer UV/visible spectrophotometer (Lambda 25/35/45, Waltham, MA, USA; <http://www.perkinelmer.com/>). Standard quartz cuvettes with a path length of 1 cm were used. Au/MNP and probe-conjugated Au/MNP morphologies were analyzed through transmission electron microscopy (TEM; Hitachi-700, Hitachi Co., Japan; <http://www.hitachi-hightech.com/>) and atomic force microscopy (AFM; Solver P47H-PRO, NT-MDT Moscow, Russia; <http://www.ntmdt-si.com/>), respectively. The TEM sample was prepared by depositing few Au colloid drops on

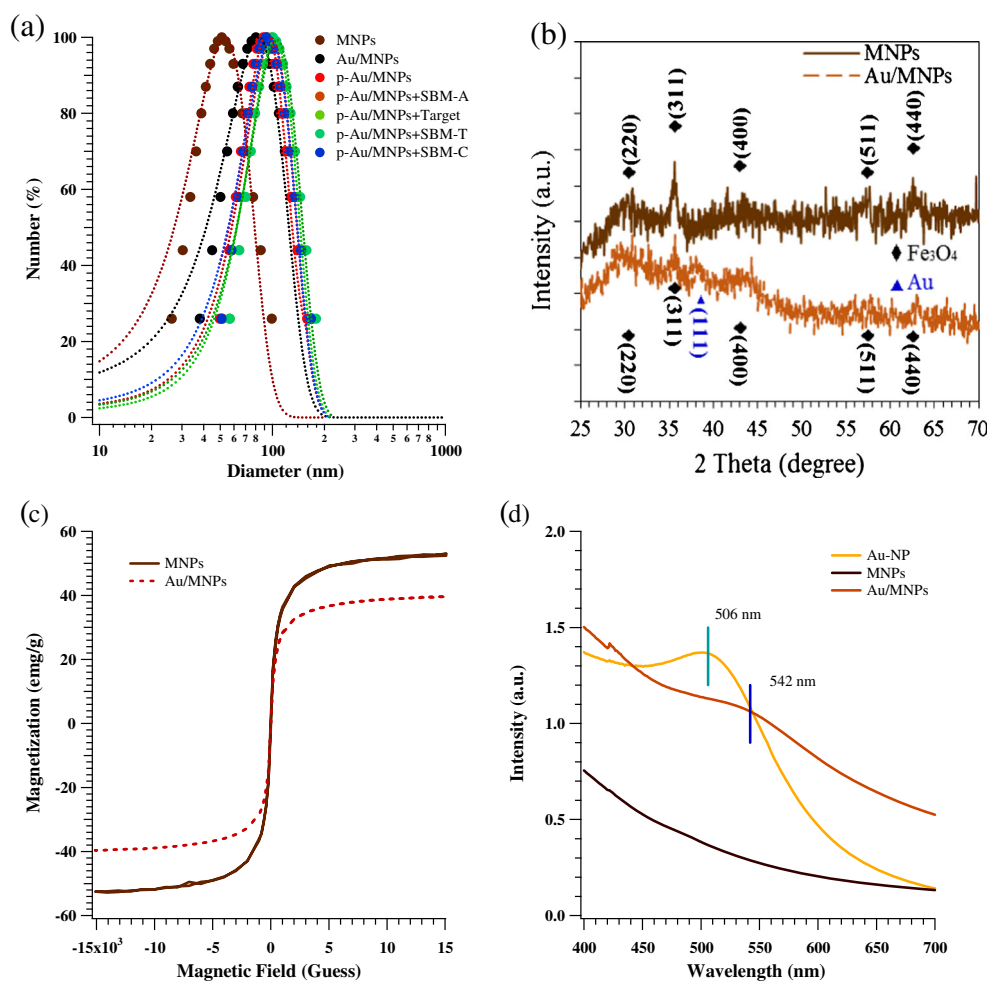
a copper grid covered with a holey carbon film. The DNA probe-conjugated Au/MNPs were freeze dried. The cantilever for AFM was a golden silicon probe (NSG01, NT-MDT; <http://www.ntmdt-si.com/>) with 6-nm probe tip and 144-kHz resonant frequency.

Measurement of fluorescence changes with DNA probe conjugation and various targets

A DNA probe of $1 \mu\text{M}$ in 3.5 mL PBS was added to 0.1 mg mL^{-1} of 3.5 mL Au/MNPs solution in a 15-mL centrifuge tube and then mixed for 30 min by vortex at room temperature. Au/MNPs were kept on the tube wall using a magnet and then the buffer (c.a. 7 mL) was removed. Probe-conjugated Au/MNPs were rinsed with PBS to remove unbound probes. Finally, the same amount of PBS was added to the probe-conjugated Au/MNPs solution to obtain the concentration of 0.05 mg mL^{-1} .

For characterization of DNA hybridization, 1 mL of the aforementioned probe-conjugated Au/MNPs was placed in a 2.5-mL cuvette without and with various concentrations of

Fig. 1 a DLS, b XRD, c SQUID, and d UV adsorption of MNPs and Au/MNPs in different conditions



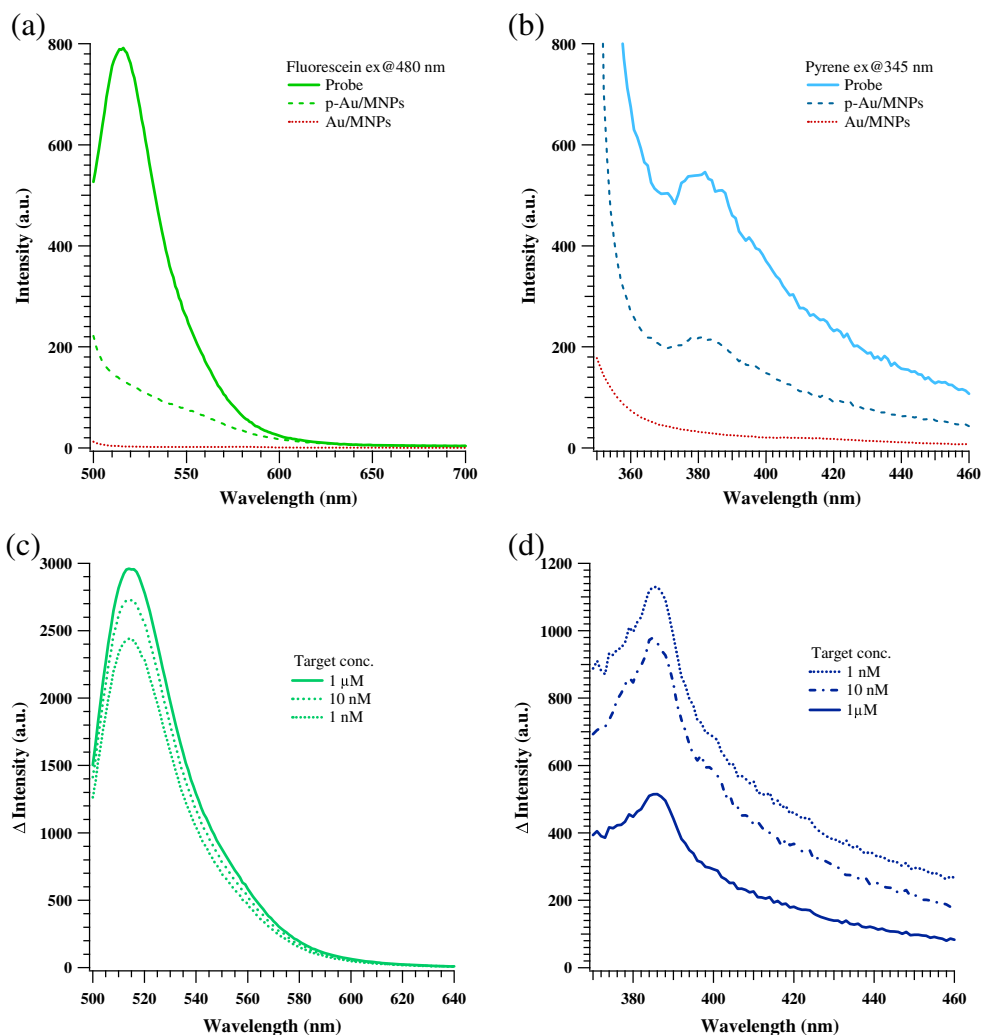
target, SBM-C, SBM-A, and SBM-T solution and monitored using a fluorescence spectrophotometer (F7000, Hitachi High-Technologies, Japan; <http://www.hitachi-hightech.com/>). The excitation and emission wavelengths were, respectively, 480/520 nm for fluorescein and 345/375 nm for pyrene. The peak bandwidths were approximately ± 20 to ± 25 nm. The relative intensities of the samples were calculated using $\Delta I = I_{\text{sample}} - I_{\text{control}}$, where I_{sample} and I_{control} are the fluorescence intensities of the target sequences and PBS (control), respectively.

For high through screening of the SNPs, the aforementioned 100 μL probe-conjugated Au/MNPs solution was placed in 96-well microplates, and various concentrations of target, SBM-C, SBM-A, and SBM-T solution (50 μL) were added and then kept stationary for 30 min for hybridization. The fluorescence intensities of excitation and emission for fluorescein (480/520 nm) and pyrene (345/375 nm) were measured using a multimode microplate reader (CLARIOstar, BMG Labtech, Germany; <https://www.bmglabtech.com/>).

Results and discussion

Several experiments were conducted to characterize the Au/MNPs. Figure 1a illustrates the size distribution of MNPs, Au/MNPs, and probe-conjugated Au/MNPs and hybridized target, SBM-C, SBM-A, or SBM-T with probe-conjugated Au/MNPs, all measured through DLS. The mean sizes of MNPs, Au/MNPs, and probe-conjugated Au/MNPs were 55, 89, and 94 nm, respectively. After adding DNA sequences (Table 1) to the probe-conjugated Au/MNPs for 30 min, the mean particle sizes with different sequences were found to be 99, 98, 104, and 107 nm, respectively, for SBM-A, SBM-C, target, and SBM-T with probe-conjugated Au/MNPs. Figure 1b shows the XRD patterns of the NPs collected and dried from completely rinsed NP solutions. MNP diffraction peaks are consistent with the standard magnetite structure pattern (JCPDS no. 79-0417). The sample demonstrates somewhat broad peaks, indicating the fineness and small crystalline size of the MNPs. Compared with MNPs, an additional peak corresponding to the (111) plane of Au (JCPDS no. 04-0784)

Fig. 2 **a** Fluorescein emissions at 520 nm and **b** pyrene-hooked pyrrocytidine for the probe alone (blue), probe attached to Au/MNPs (red), and Au/MNPs alone (green). **c** Fluorescein emissions at 520 nm and **d** pyrene-hooked pyrrocytidine with various concentrations of DNA sequence added to the composite nanoparticles



was observed in the diffraction spectrum of the core–shell Au/MNP (MNP@Au) specimen, suggesting that Au was present within the NP composite. To enhance their surface area and magnetization, the MNPs and Au/MNPs were freeze dried. Figure 1c illustrates MNP and Au/MNP magnetization. The superparamagnetic property of the MNPs was retained in the Au/MNP; however, compared with MNPs, magnetization of Au/MNP was reduced by approximately 25% (from 52.1 to 39.7 emu·g⁻¹ under a 15,000 Oe magnetic field). Figure 1d shows the UV/visible absorption spectra of the NP solutions. The SPR absorption peak of aqueous Au-NPs was observed at 506 nm, corresponding to the nanosize of NPs. However, no clear absorption peak of the pure MNP solution can be observed. The core–shell Au/MNPs solution demonstrated a much broader absorption peak at 542 nm. Because an absorption peak was observed only for the Au-NPs, the peak's redshift from 506 to 542 nm suggests Au-NP growth during or after their attachment to the Fe₃O₄ surface. Fig. S1 illustrates particles prepared at different stages: Fig. S1 (a–e) illustrates the MNPs (wine red), aqueous Au-NPs (inset TEM indicates particle size 3–5 nm), Au/MNPs, aggregation on applying magnetic field outside an Au/MNP-containing bottle, and the corresponding 3D topology of the AFM image at 100 × 100 μm². The average roughness (Sa) was approximately 363 nm, indicating Au/MNP aggregation after freeze drying.

We further tested the feasibility of the probe-conjugated Au/MNPs combination. Figure 2a shows the fluorescence intensities of fluorescein emission at 520 nm under three conditions: (i) a green line nearly on the *x*-axis, implying no emission intensity for Au/MNP alone; (ii) a red line showing a low intensity for the Au/MNP attached to the probe sequence, wherein fluorescein emission is quenched by the Au surface; and (iii) a blue line for the free probe sequence alone, wherein fluorescein is unquenched and shows a measurable peak intensity of approximately 800 au at 520 nm. The three curves in Fig. 2b are for pyrene-hooked pyrrolocytidine emission at 375 nm observed under the same conditions: (i) green line for Au/MNPs alone, with no emission intensity; (ii) red line for the probe sequence attached to Au/MNPs, with an observable emission; and (iii) blue line for the free probe sequence alone, with an observable emission. The probe sequence remained in the hairpin conformation under all these conditions, and accordingly, the pyrene microenvironment remained unchanged, so that pyrene emission can be observed. Furthermore, the probe sequence was conjugated onto the Au/MNPs, and a target sequence was added at different concentrations, from 1 nM to 1 μM, to observe how fluorescein and pyrene emission intensities varied. Figure 2c illustrates that as the added target sequence concentration increased, more probe sequences changed from a hairpin conformation to a linear duplex form, with increasing fluorescein emission intensity. Figure 2d shows that with the addition of more target sequence, the pyrene moiety became more

embedded in the matching base G, thus reducing pyrene emission intensity.

Four DNA sequences are presented in Table 1, and each sequence is 25 nt in length and in the same nucleotide sequence except for one mismatched base at a designated polymorphic site corresponding to the pyrene-labeled C* site of the probe. All the target sequences can be recognized by the 25-nt loop region of the probe sequence. Figure 3a illustrates the fluorescein intensity measured in response to the added DNA sequences. Regardless of whether the added sequences carried G for target or single-base mismatch nucleotides (e.g., SBM-C, SBM-A, or SBM-T) at the polymorphic site, the added target sequence transformed the probe sequence from a hairpin-shaped to a linear form and restored the fluorescein

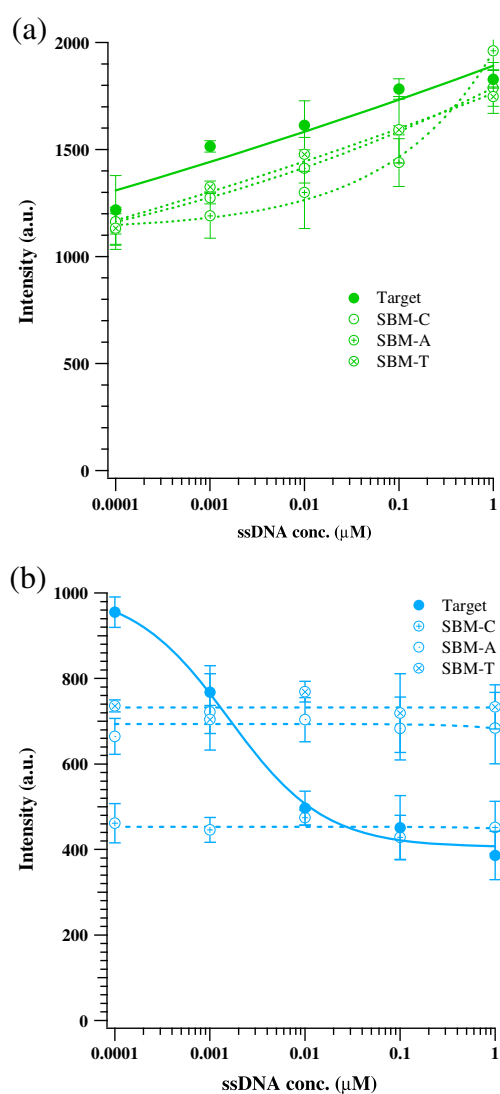


Fig. 3 Hybridization of probe-conjugated Au/MNPs with various concentrations of target, SBM-C, SBM-A, and SBM-T sequences. **a** The excitation and emission wavelengths of fluorescein are 494 and 522 nm, respectively. **b** The excitation and emission wavelengths of pyrene are 345 and 375 nm, respectively

Table 2 Overview of recently reported nanomaterial-based methods for discrimination of DNA

Materials	Method	LODs and specificity	References.
Au NPs	Bare-eye and spectrophotometric	<10 pM; unspecific	[31]
Ta ₂ NiS ₅ nanosheets	Fluorometric	50 pM; target	[32]
Au NPs	Colorimetric	0.6 pM; target/no target	[33]
Au surface	Localized surface plasmon resonance	10 nM; single-base mutations	[34]
MoS ₂ nanosheets	Spectrophotometric	315 pM; single-nucleotide polymorphism	[35]
Au/MNPs	Fluorometric	100 pM; single-base mismatch	This work

signal. The four curves indicate that the probe's concentration-dependent sensitivity to the four target sequences was approximately 0.1 nM to 1 μ M. Figure 3b illustrates the pyrene emission intensities when different DNA sequences were added. Adding target sequence, with a negative linear correlation, indicates that pyrene intensity was gradually quenched by G at the polymorphic site, in response to the target concentration. Concentration-dependent sensitivity was also observed between 0.1 nM and 1 μ M of the added target sequence. Adding SBM-C, SBM-A, and SBM-T sequences illustrates that pyrene intensities were insensitive to these added DNA sequences because these non-G nucleotides at the polymorphic site were weak pyrene quenchers.

Pyrene's fluorescence emission mainly depends on its microenvironmental polarity; a pyrene moiety placed in a polar environment, such as a DNA minor or major groove, exhibits a higher emission but a lower emission when embedded in an apolar DNA duplex core [27]. Moreover, pyrene's neighboring nucleotide affects its fluorescence emission intensity. Compared with cytosine (C), adenine (A), or thymine (T), G is a strong pyrene quencher through a photoinduced electron transfer (PET) mechanism, wherein electron transfer from the base G in close proximity to the excited pyrene moiety blocks pyrene emission [28]. The PET mechanism between G and pyrene and the discrimination of G (i.e., the target sequence) and non-G (i.e., SBM-C, SBM-A, or SBM-T sequences) can be recognized according to the off or on state of the pyrene emission [29].

The recently reported nanomaterial-based methods for the discrimination of DNA is listed in Table 2. Au surfaces are frequently used as the substrate for both immobilizations of probe and signal production. The lower LOD is found for nonspecific DNA detection than for SNP DNA detections. These DNA detection methods can achieve as low as pM; however, the LOD for SNP DNA discrimination is approximately one order higher than that for nonspecific DNA detection. The linear range of hybridization in these Au/MNPs is from 0.1 nM to 1.0 μ M of ssDNA. Moreover, the on/off signal patterns can be used to precisely tell the background, fully matched, and one-base matched outputs. With the manipulation of MNPs under the magnetic field, the LOD or linear range can be improved.

Conclusion

Au surface not only enhances stability under physiological conditions but also prevents the formation of harmful free radicals and provides surface binding of the ligand [30]. The decoration of Au NPs on the MPNs offers the manipulation of the sample handling, for example, the separation from unbound molecules, and even sample/signal concentration. Moreover, Au/MNPs have high specific surface to conjugate the SNP probe to achieve the LOD as low as pM. The design of SNP probes relies on only one signal to report fully matched and one-base mismatched DNA sequences, and either of the two outputs is likely to share the same signal pattern of the background condition. The probe proposed herein is composed of two fluorophores; their on/off patterns depend on their microenvironments. We created three on/off signal patterns to stand for the background, fully matched, and one-base matched outputs so that the false positive detection can be reduced. Given these advantages, we expect the demonstrated system can contribute to the development of SNP detection.

Acknowledgements The authors thank the Ministry of Science and Technology, Taiwan (grant nos. MOST 106-2314-B-390-001-MY2, MOST 104-2113-M-002-019-MY2, and MOST 104-2113-M-390-003) and Armed Forces Zuoying General Hospital (grant no. ZBH 105-03) for their support.

Publisher's Note Springer Nature remains neutral with regard to jurisdictional claims in published maps and institutional affiliations.

References

- Guo S, Wang E (2007) Synthesis and electrochemical applications of gold nanoparticles. *Anal Chim Acta* 598(2):181–192
- Homberger M, Simon U (2010) On the application potential of gold nanoparticles in nanoelectronics and biomedicine. *Philosophical Transactions of the Royal Society of London A: Mathematical, Physical and Engineering Sciences* 368(1915):1405–1453
- Das M, Shim KH, An SSA, Yi DK (2011) Review on gold nanoparticles and their applications. *Toxicol Environ Heal Sci* 3(4):193–205
- Daraee H, Eatemadi A, Abbasi E, Fekri Aval S, Kouhi M, Akbarzadeh A (2016) Application of gold nanoparticles in

- biomedical and drug delivery. *Artificial cells, nanomedicine, and biotechnology* 44(1):410–422
5. Wu W, Wu Z, Yu T, Jiang C, Kim W-S (2015) Recent progress on magnetic iron oxide nanoparticles: synthesis, surface functional strategies and biomedical applications. *Sci Technol Adv Mater* 16(2):023501
 6. Lee M-H, Thomas JL, Ho M-H, Yuan C, Lin H-Y (2010) Synthesis of magnetic molecularly imprinted poly (ethylene-co-vinyl alcohol) nanoparticles and their uses in the extraction and sensing of target molecules in urine. *ACS Appl Mater Interfaces* 2(6):1729–1736
 7. Lee M-H, Thomas JL, Chen Y-C, Wang H-Y, Lin H-Y (2012) Hydrolysis of magnetic amylose-imprinted poly(ethylene-co-vinyl alcohol) composite nanoparticles. *ACS Appl Mater Interfaces* 4(2): 916–921. <https://doi.org/10.1021/am201576y>
 8. Lee M-H, Thomas JL, Wang H-Y, Chang C-C, Lin C-C, Lin H-Y (2012) Extraction of resveratrol from *Polygonum cuspidatum* with magnetic orcinol-imprinted poly (ethylene-co-vinyl alcohol) composite particles and their in vitro suppression of human osteogenic sarcoma (HOS) cell line. *J Mater Chem* 22(47):24644–24651
 9. Lee M-H, Thomas JL, Chen J-Z, Jan J-S, Lin H-Y (2016) Activation of tumor suppressor p53 gene expression by magnetic thymine-imprinted chitosan nanoparticles. *Chem Commun* 52(10): 2137–2140. <https://doi.org/10.1039/C5CC09896C>
 10. Lee M-H, Ahluwalia A, Chen J-Z, Shih N-L, Lin H-Y (2017) Synthesis of magnetic cytosine-imprinted chitosan nanoparticles. *Nanotechnology* 28(8):085705
 11. Luo J, Fan Q, Suzuki M, Suzuki IS, Engelhard MH, Lin Y, Kim N, Wang JQ, Zhong CJ (2005) Monodispersed Core–Shell Fe₃O₄@Au nanoparticles. *J Phys Chem B* 109(46):21593–21601. <https://doi.org/10.1021/jp0543429>
 12. Felber M, Alberto R (2015) 99m Tc radiolabelling of Fe₃O₄-Au core-shell and Au-Fe₃O₄ dumbbell-like nanoparticles. *Nanoscale* 7(15):6653–6660
 13. Xu ZC, Hou YL, Sun SH (2007) Magnetic core/shell Fe₃O₄/Au and Fe₃O₄/Au/Ag nanoparticles with tunable plasmonic properties. *J Am Chem Soc* 129(28):8698–8699
 14. Xu CJ, Xie J, Ho D, Wang C, Kohler N, Walsh EG, Morgan JR, Chin YE, Sun SH (2008) Au-Fe₃O₄ dumbbell nanoparticles as dual-functional probes. *Angew Chem Int Ed* 47(1):173–176
 15. Nguyen TT, Mammeri F, Ammar S (2018) Iron oxide and gold based magneto-Plasmonic nanostructures for medical applications: a review. *Nanomaterials* 8(3):149
 16. Stafford S, Serrano Garcia R, Gun'ko YK (2018) Multimodal magnetic-Plasmonic nanoparticles for biomedical applications. *Appl Sci* 8(1):97
 17. Kakwre H, Materia ME, Curcio A, Prato M, Sathya A, Nitti S, Pellegrino T (2018) Dually responsive gold-iron oxide heterodimers: merging stimuli-responsive surface properties with intrinsic inorganic material features. *Nanoscale* 10(8):3930–3944. <https://doi.org/10.1039/C7NR06726G>
 18. Freitas M, Sá Couto M, Barroso MF, Pereira C, Delos Santos ÁN, Miranda-Ordieres AJ, Lobo-Castañón MJ, Delerue-Matos C (2016) Highly monodisperse Fe₃O₄@ Au superparamagnetic nanoparticles as reproducible platform for genosensing genetically modified organisms. *Acs Sensors* 1(8):1044–1053
 19. Li F, Yu Z, Zhao L, Xue T (2016) Synthesis and application of homogeneous Fe₃O₄ core/Au shell nanoparticles with strong SERS effect. *RSC Adv* 6(13):10352–10357
 20. Liu X, Yang X, Xin H, Tang X, Weng L, Han Y, Geng D (2016) Ecofriendly fabrication of Au/Fe₃O₄-chitosan composites for catalytic reduction of methyl orange. *J Mater Chem B* 4(12):2337–2348
 21. Kaur M, Pramanik S, Kumar M, Bhalla V (2017) Polythiophene-encapsulated bimetallic Au-Fe₃O₄ Nano-hybrid materials: a potential tandem photocatalytic system for nondirected C(sp²)-H activation for the synthesis of Quinoline carboxylates. *ACS Catal* 7(3): 2007–2021
 22. Lin FH, Doong RA (2017) Catalytic Nanoreactors of Au@ Fe₃O₄ yolk-shell nanostructures with various Au sizes for efficient Nitroarene reduction. *J Phys Chem C* 121(14):7844–7853
 23. Zhou H, Lee J, Park TJ, Lee SJ, Park JY, Lee J (2012) Ultrasensitive DNA monitoring by Au-Fe₃O₄ nanocomplex. *Sensors Actuators B Chem* 163(1):224–232
 24. Du H, Disney MD, Miller BL, Krauss TD (2003) Hybridization-based unquenching of DNA hairpins on Au surfaces: prototypical "molecular beacon" biosensors. *J Am Chem Soc* 125(14):4012–4013. <https://doi.org/10.1021/ja0290781>
 25. Shiddiky MJ, Shim Y-B (2007) Trace analysis of DNA: preconcentration, separation, and electrochemical detection in microchip electrophoresis using Au nanoparticles. *Anal Chem* 79(10): 3724–3733
 26. Heim T, Preuss S, Gerstmayr B, Bosio A, Blossey R (2005) Deposition from a drop: morphologies of unspecifically bound DNA. *J Phys Condens Matter* 17(9):S703–S716
 27. Okamoto A, Saito Y, Saito I (2005) Design of base-discriminating fluorescent nucleosides. *Journal of Photochemistry and Photobiology C-Photochemistry Reviews* 6(2–3):108–122. <https://doi.org/10.1016/j.jphotochemrev.2005.07.002>
 28. Saito Y, Shinohara Y, Bag SS, Takeuchi Y, Matsumoto K, Saito I (2008) Design of an ultimate quencher free molecular beacon containing pyrrolocytidine-guanine base pair. *Nucleic Acids Symp Ser (Oxf)* 52:361–362. <https://doi.org/10.1093/nass/nm182>
 29. Lee MH, Lin HY, Chang HW, Yang CN (2018) Detection of DNA sequences with a single-base mismatch on a gold-based and pyrene-assisted platform. *Sensors and Actuators B-Chemical* 266:522–527. <https://doi.org/10.1016/j.snb.2018.03.096>
 30. Salihov SV, Ivanenkov YA, Krechetov SP, Veselov MS, Sviridenkova NV, Savchenko AG, Klyachko NL, Golovin YI, Chufarova NV, Beloglazkina EK (2015) Recent advances in the synthesis of Fe₃O₄@ Au core/shell nanoparticles. *J Magn Magn Mater* 394:173–178
 31. Lepoitevin M, Lemouel M, Bechelany M, Janot J-M, Balme S (2015) Gold nanoparticles for the bare-eye based and spectrophotometric detection of proteins, polynucleotides and DNA. *Microchim Acta* 182(5):1223–1229. <https://doi.org/10.1007/s00604-014-1408-1>
 32. Tan C, Yu P, Hu Y, Chen J, Huang Y, Cai Y, Luo Z, Li B, Lu Q, Wang L, Liu Z, Zhang H (2015) High-yield exfoliation of ultrathin two-dimensional ternary chalcogenide Nanosheets for highly sensitive and selective fluorescence DNA sensors. *J Am Chem Soc* 137(32):10430–10436. <https://doi.org/10.1021/jacs.5b06982>
 33. Zeng Y, Zhang D, Qi P, Zheng L (2017) Colorimetric detection of DNA by using target catalyzed DNA nanostructure assembly and unmodified gold nanoparticles. *Microchim Acta* 184(12):4809–4815. <https://doi.org/10.1007/s00604-017-2463-1>
 34. Rapisarda A, Giambanco N, Marletta G (2017) Kinetic discrimination of DNA single-base mutations by localized surface plasmon resonance. *J Colloid Interface Sci* 487:141–148. <https://doi.org/10.1016/j.jcis.2016.10.026>
 35. Li BL, Zou HL, Lu L, Yang Y, Lei JL, Luo HQ, Li NB (2015) Size-dependent optical absorption of layered MoS₂ and DNA oligonucleotides induced dispersion behavior for label-free detection of single-nucleotide polymorphism. *Adv Funct Mater* 25(23):3541–3550. <https://doi.org/10.1002/adfm.201500180>